Supplementary Information

Overprinting with Tomographic Volumetric Additive Manufacturing

Felix Wechsler[1,*], Viola Sgarminato[1,2], Riccardo Rizzo[1], Baptiste Nicolet[3,4], Wenzel Jakob[3,*], Christophe Moser[1,*]

[1]Laboratory of Applied Photonics Devices, École polytechnique fédérale de Lausanne (EPFL), Lausanne, Switzerland
[2]BIOINSIDE Lab, Department of Mechanical and Aerospace Engineering, Politecnico di Torino, Italy
[3]Realistic Graphics Lab, École polytechnique fédérale de Lausanne (EPFL), Lausanne, Switzerland
[4]NVIDIA, Zürich, Switzerland

[*]Corresponding authors:
overprinting@felixwechsler.science,
wenzel.jakob@epfl.ch,
christophe.moser@epfl.ch

May 5, 2026

A Lenses on test tube

In this experiment, we demonstrate printing a lens onto a cylindrical glass tube filled with water. The lens is designed to image samples immersed in the water inside the tube. As in the previous examples,

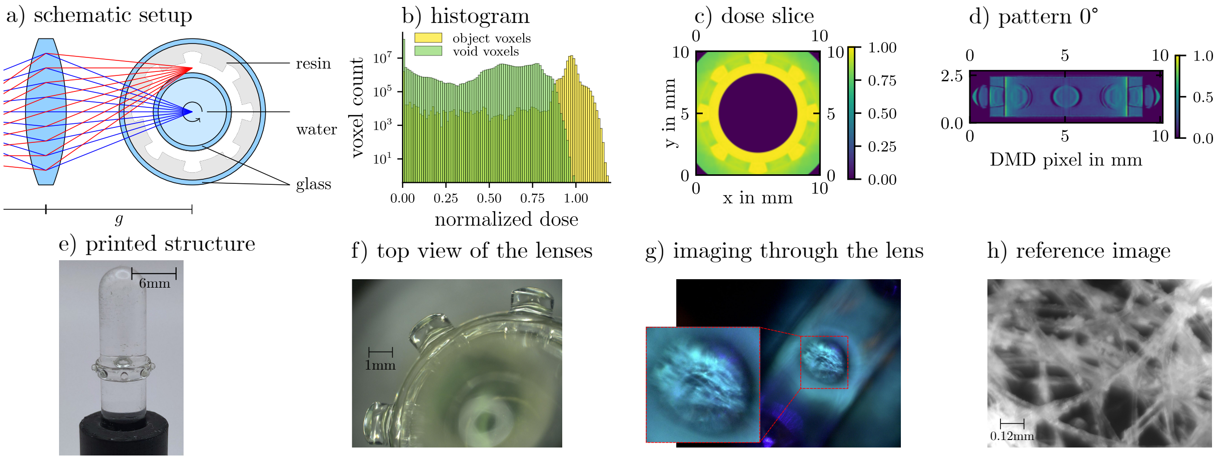

Figure S1: Printing a lens on a water-filled glass cuvette for in-situ imaging. a) Schematic of the experimental setup. b) Voxel dose histogram from the simulation. c) A slice of the cumulative dose map. d) Example projection patterns from two different angles. e) The final printed lens on the cuvette. f) Top view of the lenses on the cuvette. g) Illustration of the lens's intended function for imaging a sample within the tube. h) A reference image of the same sample.

the optical paths are complex due to the multiple media involved in the light propagation. The embedded water, in particular, has negligible absorption but a refractive index that differs significantly from the other materials. Therefore, it is crucial to account for the multiple refractions occurring at the interfaces between vial, resin, small vial, and water.

A schematic of the setup is shown in Figure S1a). Optimizing the patterns for this geometry yields the histogram in Figure S1b) and a dose slice in Figure S1c). Some object voxels fall within the water-filled cuvette; while these are not printed, they contribute to the apparent discrepancies in the histogram. One example pattern is shown in Figure S1d).

The final printed lens structure on the inner glass cuvette is shown in Figure S1e), with a detailed view in Figure S1f). The lens is designed to image samples placed inside the water-filled tube. As a sample we used optical tissue paper, which was stained with text marker. We subsequently used its qualitative working principle as shown in Figure S1g). A similar reference image of the sample is presented with a 4× microscope in Figure S1h). The contrast is low because the tissue was embedded in water and the fluorescent marker diffused into the water and contributes to background light. A test tube with an inner radius of $r_{\text{inner}} = 2.58\,\text{mm}$, an outer radius of $r_{\text{outer}} = 3.18\,\text{mm}$, and a refractive index of 1.54 was used as the substrate to print on. The tube was filled with water and secured in the center of the larger printing vial using an SLA-printed cap. The microlenses were designed to image the central axis of the test tube.

B Dice on mirror

In this section we demonstrate printing onto a smooth mirrored surface. The general setup for this print is shown in Figure S2a). Because of the internal reflection the ray-path is complex as qualitatively shown. We fabricated the cuvettes by gluing custom cut mirrors on the inside of the square cuvette. An example cuvette filled with resin is displayed in Figure S2b). This arrangement implies that there is a glass layer on top of the mirror. We model all interfaces and reflection with our software Dr.TVAM.

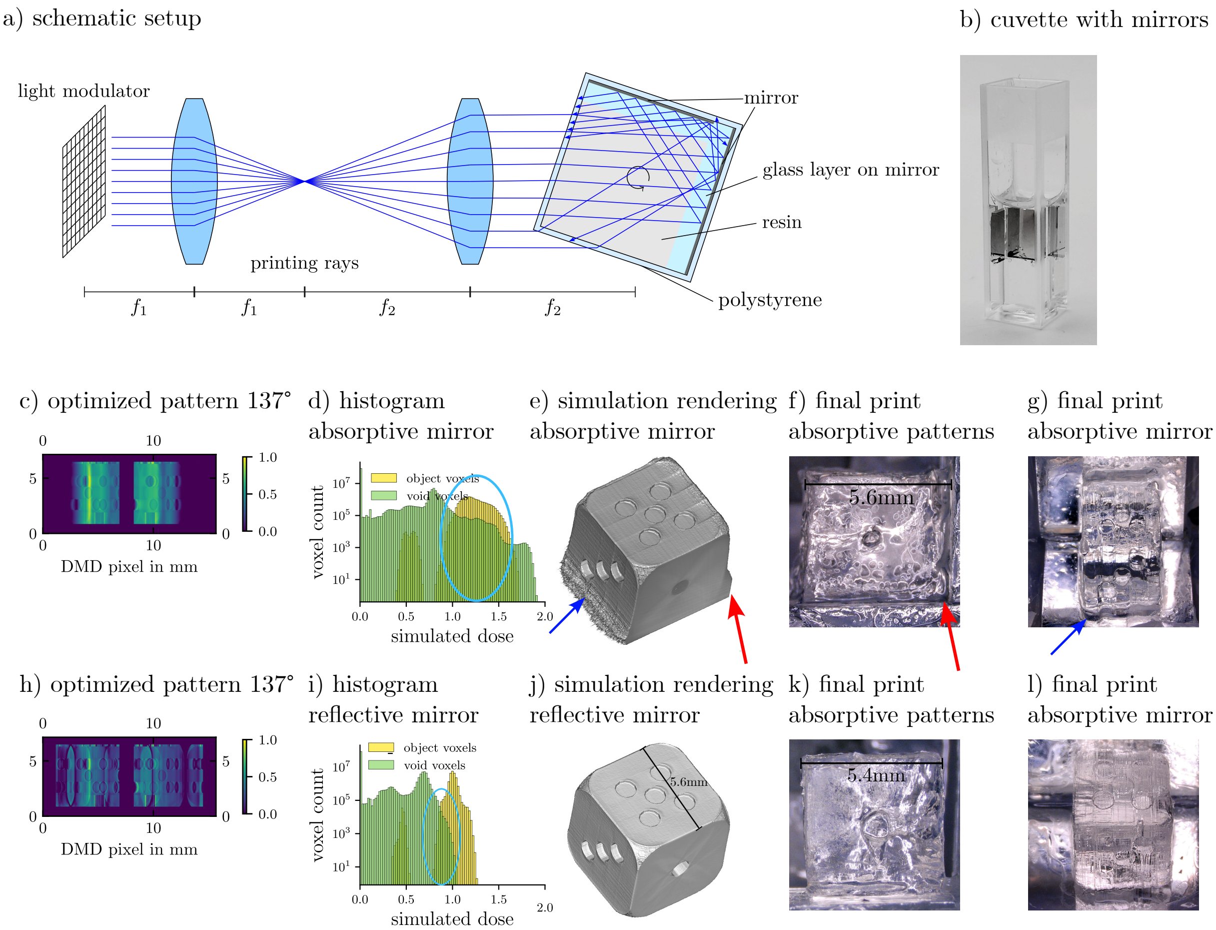

Figure S2: Overprinting of a dice onto a reflective mirro surface. a) schematic experimental setup. b) two mirrors glued into a quadratically shaped cuvette. c) optimized patterns for absorbing mirrors. d) dose histogram for patterns with absorbing mirrors projected onto reflecting mirrors. e) best simulation rendering for that case. f) experimental print of absorbing patterns on reflective mirror. g) experimental print of absorbing patterns on reflective mirror. h) optimized patterns for reflective mirrors. i) dose histogram for patterns with reflective mirrors. j) best simulation rendering for that case. k) experimental print of reflective patterns. l) experimental print of reflective patterns.

To showcase our software, we compare two scenarios. The first scenario assumes that the mirror is fully light absorbing. One specific pattern of the optimization is in Figure S2c). If we project those patterns, we already identify a certain overlap in the histogram in Figure S2d) (marked by the blue ellipsis). Also, the 3D rendering of the best possible theoretical print in Figure S2e) shows some deformations from an ideal cube. Further, our experimental prints with the absorptive patterns show some deformations in Figure S2f) and g). See the red arrow for the most severe discrepancies. The gap between one of the mirrors and the cube is closed, even though by design it should not be. There is also a edge artefact on one side (blue arrow).

In our framework we can correctly simulate patterns with a large amount of reflection, as seen in Figure S2h) where multiple reflections of the mirrors can be observed. The histogram in Figure S2i) displays higher fidelity. The final rendering of the reflection aware patterns is in Figure S2j). This time, the overall quality is slightly higher and the gap between the second mirror is preserved. The final, well preserved prints are shown in Figure S2k) and l).

C Rendering of the channels

Figure S3 contains a Blender rendering of the printed channels of the perfusable chips. The black caps at the top and bottom were SLA fabricated and contain the nozzle inlets.

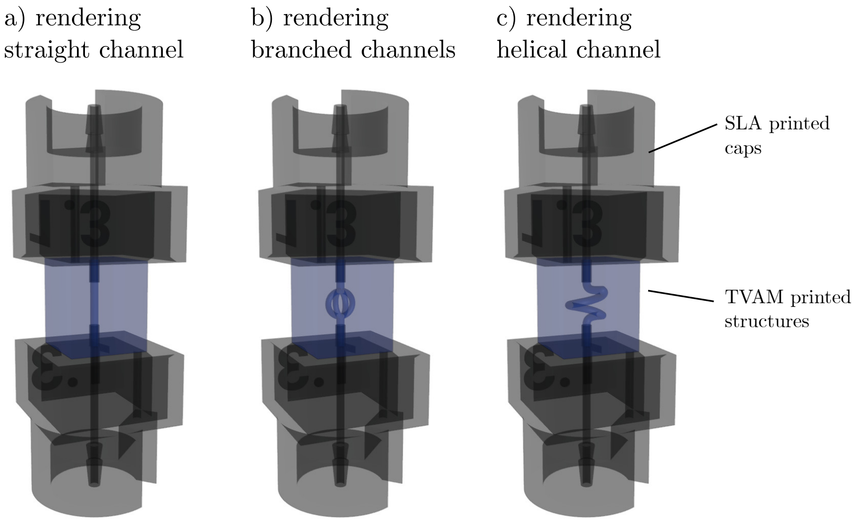

Figure S3: Rendering of the TVAM printed channels with SLA printed caps. a) straight channel, b) branched channels and c) helical channel.

Note, we did not render the square cuvette itself since this is not modelled with a mesh file but instead is handled by our software Dr.TVAM.

D Exposure series

To rule out the possibility that the visible defects in Figure 3 for the gear printed from the uncorrected pattern are caused by operator-induced under- or overexposure, we present an exposure series in Figure S4. The top row shows prints obtained at different exposure powers using the uncorrected pattern, whereas the bottom row shows the corresponding results for the scattering-corrected pattern.
The fine features located close to the rod are consistently overpolymerized in the prints produced from the uncorrected pattern. Notably, even under substantial underexposure, overpolymerization persists near the rod, while the remainder of the gear is clearly underexposed.
In contrast, the holes are generally much better preserved for the scattering-corrected patterns. As this behavior is also in good agreement with the simulations, we can exclude the existence of an exposure power for the uncorrected pattern that would produce a print with well-preserved holes.

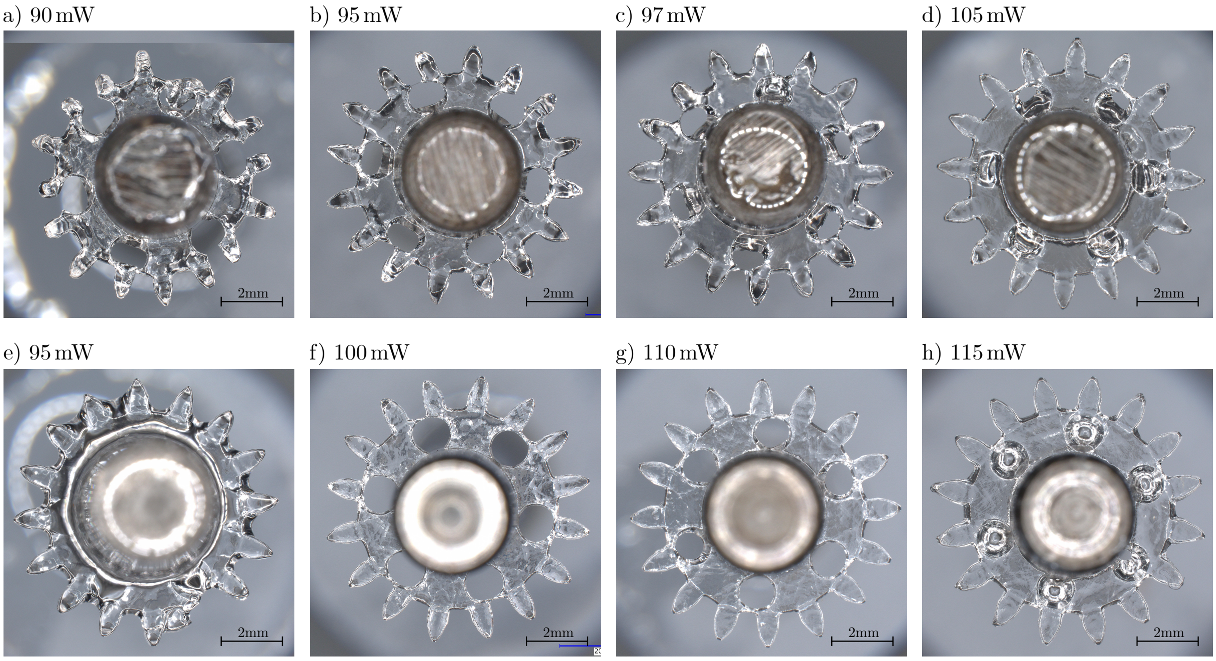

Figure S4: Exposure series for the gear structures. Top row: a)–d) prints obtained from the uncorrected pattern at different exposure powers. Bottom row: e)–h) corresponding prints obtained from the scattering-corrected pattern.

E Beckmann distribution to model a scattering rod

The Beckmann distribution is a mathematical model that describes how light scatters from rough surfaces by characterizing the statistical distribution of microscopic surface normals (microfacets). In computer graphics rendering systems like Mitsuba (which Dr.TVAM is based on), it serves as a physically-based microfacet normal distribution function (NDF) derived from Gaussian random surfaces, enabling realistic simulation of surface roughness and light reflection.

The Beckmann distribution is characterized by a single parameter α which describes how strong the light is scattered.

In our experiment, we estimated α by projecting a single pixel onto the metal rod. We embedded the rod inside a fluorescent water bath. This allows us to make the scattering light visible with a camera from below. From the spread of the reflected light we can then estimate $\alpha = 0.03$. Figure S5 shows the reflected light curves for $\alpha = 0.02$ and $\alpha = 0.04$ which show a good, but not a perfect fit. The results indicated in Figure 3b) with $\alpha = 0.03$ show a much better fit.

In Figure S6 we illustrate how a single pixel projects light (from right to left) onto a metal rod with varying values of α. The light intensity is recorded according to the absorbing medium. To make the low intensity of the scattered light visible, we show the image with a gamma correction of $\gamma = 0.5$. As it can be seen, higher values of α indeed scatter the light stronger.

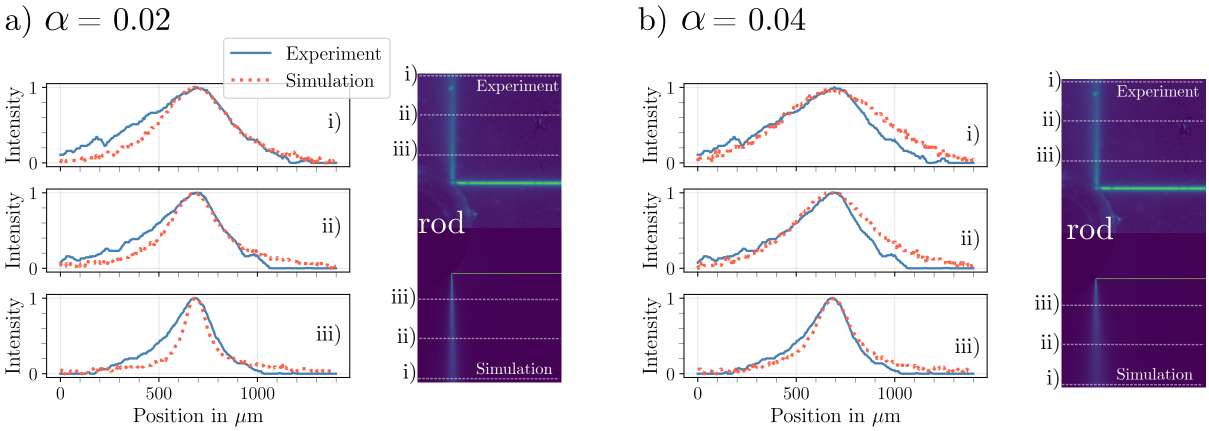

Figure S5: Characterization of the α parameter. The experimental captured image and the simulated response and three cross section at different distances to the rod. a) shows the results for $\alpha = 0.02$ and b) for $\alpha = 0.04$.

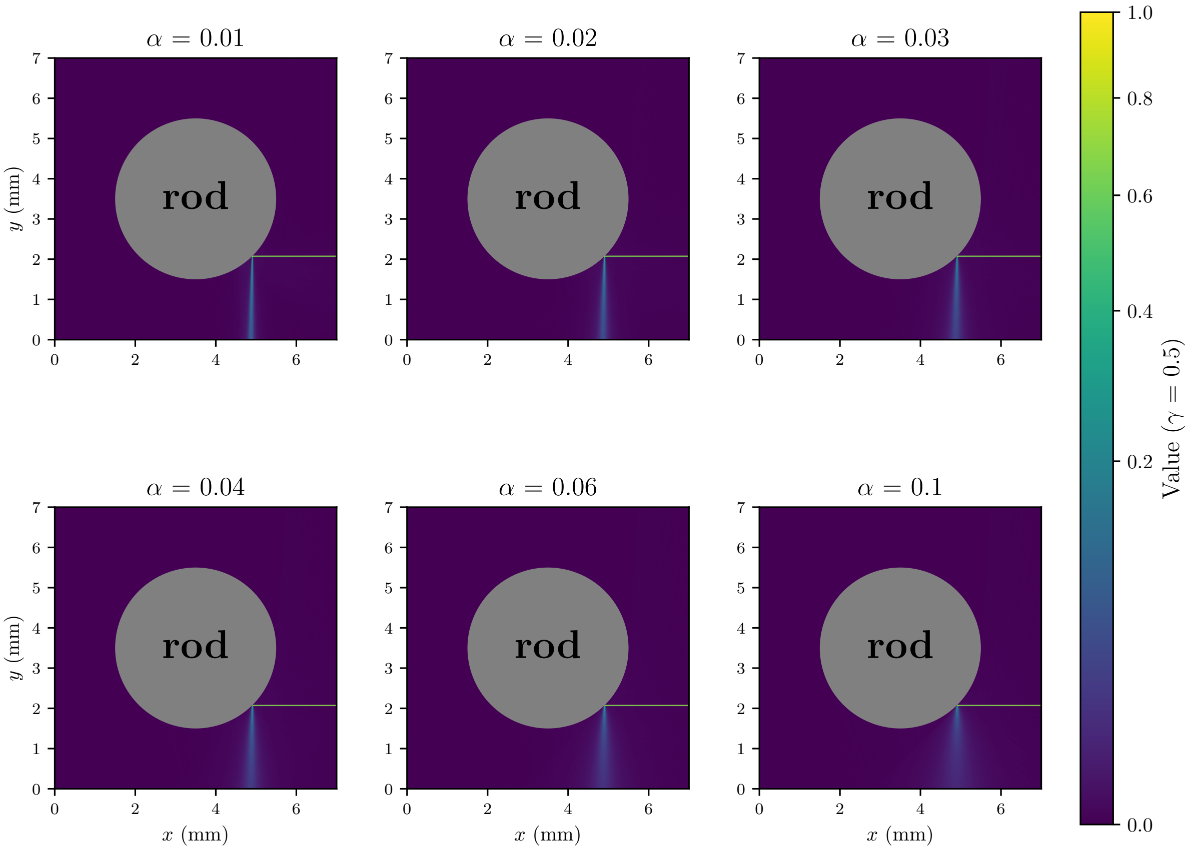

Figure S6: The deposit intensity from a single pixel illuminating the rod from the right which results in scattered paths. We show different values of α used for the Beckmann distribution from the metal rod. Note, we display the intensity applied with a gamma factor of $\gamma = 0.5$ to make the weakly scattered rays visible.

F Dose histograms

Figure S7 displays the dose histograms for the experiments in Section Context-aware perfusion system, Section Gear on metal rod and Section Optical lens with symbol on LED. Dose histograms are an effective way to judge the quality of the projection patterns. Note, all histograms are in a logarithmic scale. For example, Figure S7a), c) and d) results in high quality prints as there is no significant overlap. However, Figure S7b) shows a noticeable overlap as we apply patterns simulated in an absorptive gear case to a scattering gear. Notice, the yellow dose in Figure S7d) corresponds to voxels partially inside the LED hence they do not result in visible quality loss.

a) histogram for context-aware perfusion system — b) histogram for gear with absorptive patterns — c) histogram for gear with scattering patterns — d) histogram for LED projector

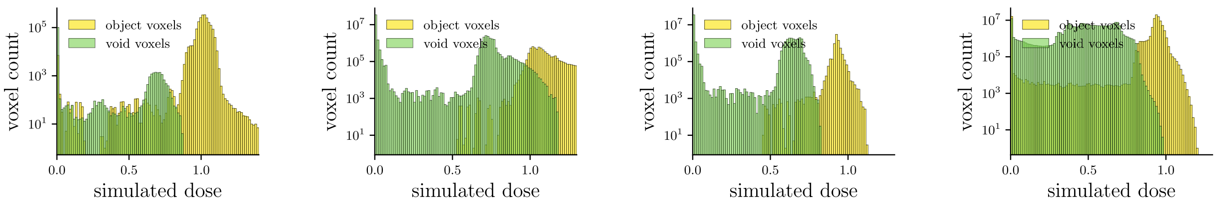

Figure S7: Simulated dose histograms for a) the context-aware perfusion system, b) the absorptive patterns for the gear applied to a scattering gear overprint, c) the scattering patterns of the gear overprinting and d) for the LED overprinting.

G Printing Parameters

This section contains the printing and optimization parameters for the experiments presented in Supplement Lenses on test tube and Supplement Dice on mirror.

Experiment	T_{opt} in s	η_{energy} in %	T_L	T_U	$w_{sparsity}$
lenses for imaging	4019	12.3	0.8	0.95	10^{-25}
absorptive mirror	1107	0.07	0.7	0.94	2
reflective mirror	1741	0.01	0.7	0.94	2

Table S1: Specifications for the pattern optimization. T_{opt} is the time required for the pattern optimization. η_{energy} indicates the energy efficiency of each set of patterns. T_L and T_U are the lower and upper thresholds, respectively, as defined in Equation 1. $w_{sparsity}$ governs the sparsity of the patterns.

Experiment	setup	P in mW/mm^2	T_{print} in s	ω in °/s	μ in 1/mm
lenses for imaging	LEDTVAM	0.33	30.0	60.0	0.11
absorptive mirror	LaserTVAM	1.22	25.2	100	0.129
reflective mirror	LaserTVAM	0.95	28.8	100	0.129

Table S2: Experimental conditions for the print. P indicates the maximum power per area available. T_{print} represents the total printing time. ω denotes the rotational speed of the stage. μ is the attenuation coefficient used for absorption.